

# Wave Haptics: Building Stiff Controllers from the Natural Motor Dynamics

Nicola Diolaiti, Günter Niemeyer, Neal Tanner

**Abstract**—Haptics, like the fields of robotics and motion control, relies on high stiffness position control of electric motors. Traditionally DC motors are driven by current amplifiers and encoder-based position feedback creates virtual springs. Unfortunately, sensor quantization, discretization, and amplifier bandwidths impose performance limits, while the amplifiers work hard to cancel the motor’s electrical dynamics.

We present an alternate approach noting the natural inductor-resistor dynamics of the motor are indeed beneficial to the haptic task. We follow two main insights: First, the electrical inductance  $L$  can serve as a stiffness, providing a natural sensorless coupling between the virtual environment and the user. This physical effect is available at all frequencies and can be exploited in the bandwidth of human perception through an analog circuit that replaces the traditional current amplifier. Second, the analog circuit uses the electrical resistance  $R$  to create a natural wave transform. Controlling the system in wave variables creates robustness to servo delays and discretization. The resulting system requires only a simple voltage drive circuit. Built upon the motor’s physical behavior, it can outperform traditional approaches, by achieving higher virtual stiffness in the range of frequencies where human users are most sensitive.

Encoder feedback and a slow digital control loop may be added to assure stable low frequency behavior and provide robustness to motor parametric uncertainty. In contrast to traditional designs, this auxiliary feedback path places reduced requirements on resolution and servo rates. A prototype 1-DOF system has been implemented and confirms the promise of this novel paradigm.

## I. INTRODUCTION

Haptic perception allows humans to gather a considerable amount of information about the mechanical properties of the objects they interact with. Several studies have analyzed the capabilities of human perception, characterizing our sensitivity to different frequencies of the contact dynamics [3], [4]. In particular, we can detect haptic stimuli up to about 1 KHz, with a sensitivity peak at about 200 Hz [5].

In order to enable the user to correctly perceive the simulated contact with virtual objects, the mechanical design and control architecture of haptic interfaces therefore have

N. Diolaiti is with DEIS, Dept. of Electronics, Computer Science and Systems of the University of Bologna, Viale Risorgimento 2, 40136, Bologna, Italy (e-mail: ndiolaiti@deis.unibo.it) and with the Stanford AI-Robotics Lab.

G. Niemeyer (corresponding author) and N. Tanner are with Stanford Telerobotics Lab, Stanford University 380 Panama Mall, Stanford, CA 94305, USA (e-mail: {gunter.niemeyer, tanner}@stanford.edu)

Subsets of this work [1], [2] have been presented at the 12th International Symposium of Robotics Research (ISRR 2005) and are accepted for presentation at the 14th Symposium on Haptic Interfaces for Virtual Environment and Teleoperator Systems (HAPTICS 2006).

The authors would like to gratefully acknowledge support for this research which was provided, in part, by NIH Grant R33 LM 007295 and by the AGI Corporation.

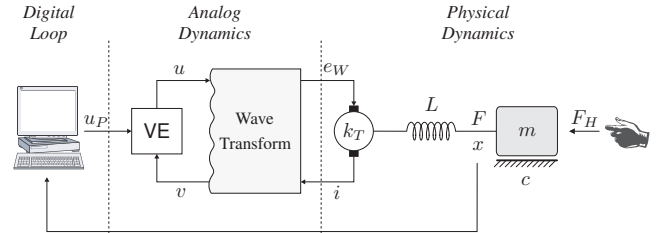


Fig. 1. The Wave Haptics approach: analog circuitry implements an energy consistent inner loop for stable interaction at high frequency. The external digital loop ensures low frequency accuracy. Motor inductance acts as elastic coupling to the user.

to account for these characteristics. Commonly, devices with impedance causality are designed to minimize their intrinsic friction and inertia [6], while the control algorithms have to guarantee a stable interaction with stiff environments over a frequency range matching the user sensitivity. In this setting, bandwidth and rate hardness [7] are common metrics to evaluate the effectiveness of haptic displays.

However, the stable implementation of stiff virtual environments over a wide range of frequencies is still a challenging problem. In fact, the interconnection between the physical domain and the virtual environment is traditionally achieved by directly sensing device position and commanding the feedback force to a current controlled actuator [8]. Maximum achievable stiffness, and consequently bandwidth and stability of the haptic interaction, is limited by the lack of information to the controller caused by time discretization [9], [10], computational delays [11] and position quantization [12], [13] from encoders. These phenomena lead to spurious energy generation and eventually instability if not dissipated through the intrinsic friction of the device, controller [14] or damping from the user’s grasp. Alternatively, the use of analog position measurements and time continuous feedback [15] has been shown to improve the dynamic range of haptic rendering [16].

In this paper we propose an alternative approach to the control of force feedback devices. First we recognize that a haptic interface acts as a transducer that transfers mechanical power, expressed by the product of force and velocity, between the mechanical domain and the virtual environment. As previously noted, such power conversion is usually implemented by means of a digital control loop. However, the fact that the DC motor itself is a transducer that couples mechanical and electrical domains in a stable fashion is often overlooked in the field of haptics. This assumption is justified by the behavior of current amplifiers, that use an internal feedback loop to

speed up the electrical dynamics while rejecting back-EMF effects, that are treated as disturbances. On the other hand, [17] showed the possibility of using electrical dynamics to increase the apparent viscous friction to improve the stability of haptic devices, while full state estimators [18] can be used in place of tachometers to derive accurate velocity measurements from the back-EMF voltage.

Second, the analysis of motor dynamics shows that the electrical inductance  $L$  provides a stiff behavior (*electrical stiffness* in the following), that is naturally available at high frequency, while at lower frequencies it is masked by the electrical resistance  $R$ . Therefore, the analog circuit sketched in Fig. 1 is proposed to replace the traditional current amplification and is designed in order to exploit the electrical stiffness over a range of frequencies that matches the user's sensitivity peak. The electrical stiffness is a physical component and is therefore passive and stable. It provides force feedback without requiring direct position sensing and hence does not suffer from poor encoder resolution. The high value of electrical stiffness for motors commonly found in haptic devices allows to surpass the performance obtained through traditional approaches. Furthermore, the analog circuit can be described in terms of wave variables [19]–[21] that provide robustness to servo delays when interfaced to a time-discrete controller.

Finally, digital control and encoder-based absolute position sensing are used to provide the necessary low frequency behavior. According to the previous discussion, user sensitivity and position resolution is relatively small in this range of frequencies. This fact allows for relaxed feedback gains in the digital loop, whose stability results therefore less critical than in the traditional scheme [13].

The paper is organized as follows: in Sect. II motor dynamics are briefly recalled and the mechanical equivalents of electrical dynamics are derived. Their potential to provide encoderless force feedback and position holding is discussed in Sect. III, while in Sect. IV we present the more general framework of wave variables that, through a simple analog circuit, allow to build the interface between electrical dynamics with virtual environments necessary for haptic rendering. To evaluate the performances of the proposed approach, in Sect. V we focus on the implementation of stiff contact and free motion. Root locus analysis in Sect. VI emphasizes differences and analogies with the traditional approach, while in Sect. VII we discuss the design of a digital control loop to provide robustness to parametric uncertainties. Overall system performances are evaluated in Sect. VIII, where we show how the approach we propose is able to stably render high stiffnesses especially at high frequency, thus matching the characteristics of the human kinesthetic perception. Finally, the experiments on a simple 1-DOF testbed, presented in Sect. IX confirm the theoretical expectations.

## II. INTERPRETING THE MOTOR DYNAMICS

Though generally ignored under the assumptions of an ideal actuator and perfect current amplification, the electrical motor

dynamics are well known to be:

$$e_A(t) = Ri(t) + L \frac{di(t)}{dt} + e_B(t) \quad (1)$$

$$e_B(t) = k_T \dot{x}(t) \quad (2)$$

where  $e_A$  is the applied voltage to the armature circuit consisting of the resistance  $R$ , the inductance  $L$  and the back-EMF voltage  $e_B$ . The mechanical dynamics are given as:

$$m\ddot{x}(t) = F(t) - c(\dot{x}(t)) - F_H(t) \quad (3)$$

$$F(t) = k_T i(t) \quad (4)$$

where  $m$  is the rotor inertia,  $c$  is the (nonlinear) friction and  $F_H$  is the user torque *opposing* the motion  $\dot{x}$  of the rotor. The torque constant and back-EMF constant are the same physical parameter and are both denoted by  $k_T$ . The dynamic system is illustrated in Fig. 2(a) and represented in block diagram form in Fig. 2(b).

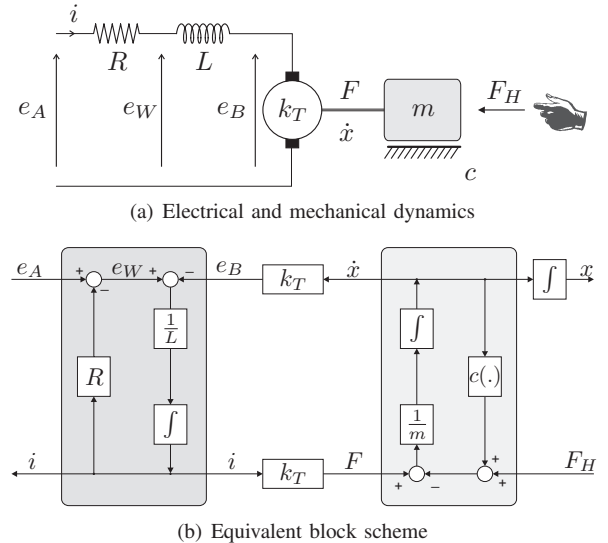


Fig. 2. DC motor dynamics and equivalent block scheme

As stated by (2) and (4), the actuator couples the mechanical and electrical domains. Hence, it is possible to take advantage of the coupling equations to interpret the electrical dynamics in the mechanical domain.

Coupling equations (2) and (4) relate torque to current and voltage to velocity. Since the inductance  $L$  sets a current proportional to the integral of its terminal voltage, it corresponds to a spring of stiffness:

$$K_L = \frac{k_T^2}{L} \quad (5)$$

which generates a torque  $F$  proportional to the integral of the net velocity of its endpoints. Similarly, the resistance  $R$  maps into a mechanical viscous damper:

$$B_R = \frac{k_T^2}{R} \quad (6)$$

As shown in Fig. 3, the equivalent spring and damper share the same torque  $F$ , hence they are connected in series between the rotor inertia and the energy conversion element, which

corresponds to a gyrator in bond graphs terms [22], [23]. Because of the series connection, the behavior is dominated by the damper in the range of frequencies of kinesthetic interaction and the stiffness is often overlooked.

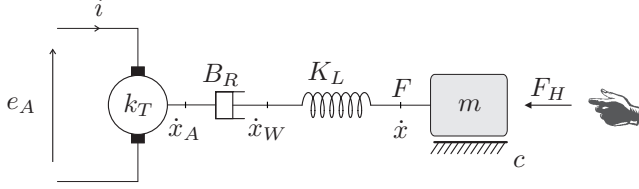


Fig. 3. Rotor inductance  $L$  and resistance  $R$  interpreted as series connection of a spring  $K_L = k_T^2/L$  and a viscous damper  $B_R = k_T^2/R$

With low inductance motors commonly used in haptics,  $K_L$  can be a very high stiffness. For example, for the Maxon RE 25 motors found in the PHANToM 1.0 with values of  $k_T = 43.8$  mNm/A and  $L = 0.83$  mH, we have  $K_L = 2.31$  Nm/rad. With an approximate 8 : 1 gear ratio and lever arm of 14 cm the corresponding tip stiffness reaches 7500 N/m. For comparison, the maximum stable value of a virtual spring implemented according to the traditional scheme has been found to be approximately 1100 N/m [13], corresponding to about 0.34 Nm/rad in joint space.

Therefore, a control scheme that treats the motor inductance as a spring in mechanical series and directly controls  $\dot{x}_W$  could stably render higher overall stiffnesses than traditional approaches. Indeed  $K_L$  is a *physical* element of the system, so it is not affected by the non-idealities of the digital control loop that cause energetic inconsistencies and lead to instability. Moreover, because velocity information is obtained through the back-EMF effect of the motor, this force feedback does not require an actual position sensor and operates naturally at high frequencies.

### III. ENCODERLESS POSITION HOLDING

We begin with the task of building a simple controller that locks the position of the motor without using explicit position sensing and feedback. Because we are attempting to directly control  $\dot{x}_W$ , we consider the inductance  $L$  to exist in the mechanical domain as  $K_L$  while retaining the resistance  $R$  in the electrical domain. This configuration is illustrated graphically and in block diagram form in Fig. 4.

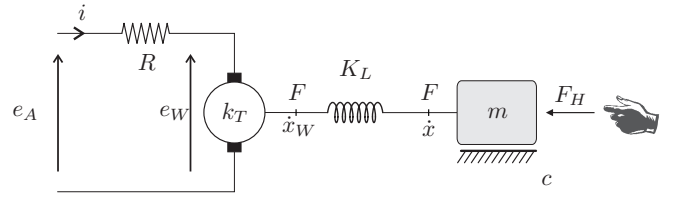
This assumption simplifies the electrical dynamics into purely algebraic relationships that can be easily controlled:

$$e_W = e_A - Ri \quad \dot{x}_W = \frac{e_W}{k_T} \quad (7)$$

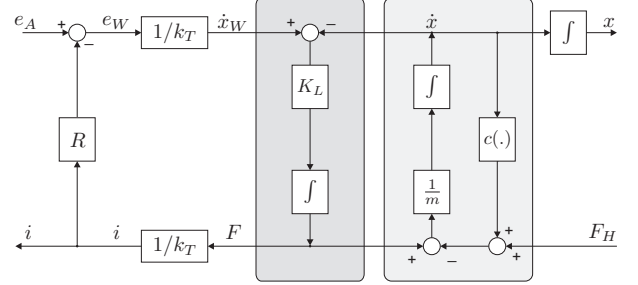
To this end, it is sufficient to design an analog voltage drive that actively compensates for motor resistance  $R$  by setting:

$$e_A = Ri \implies e_W = 0 \implies \dot{x}_W = 0 \quad (8)$$

By using knowledge of the motor's resistance to regulate the voltage across the energy conversion element to zero, we also force the velocity at the spring end-point to zero. We allow the motor inductance to provide the coupling between  $x_W$  and the actual rotor position  $x$ . The end result is that the user feels a rigid constraint through the high stiffness of  $K_L$ .



(a) System dynamics with the motor inductance in the mechanical domain



(b) Equivalent block scheme

Fig. 4. Interpretation of motor inductance as mechanical spring  $K_L$  for analog circuit design

A possible implementation based on elementary op-amp blocks is depicted in Fig. 5. A voltage proportional to the current  $i$  is derived by means of a sense resistor  $R_S$  and, through a low pass filter that is needed to attenuate high frequency noise, is fed to the compensator that amplifies it by a factor  $(R + R_S)/R_S$  (the coefficient  $\alpha$  simply scales the actual resistors to values that guarantee a good signal to noise ratio for the op-amps). The overall transfer function is:

$$E_A(s) = \frac{R + R_S}{R_S} \frac{1}{R_f C_f s + 1} R_S I(s) \quad (9)$$

and at frequencies not attenuated by the filter corresponds to (8), where the total resistance that has to be compensated is  $R + R_S$ . Finally two complementary power transistors in push-pull configuration are used to apply the commanded voltage to the motor.

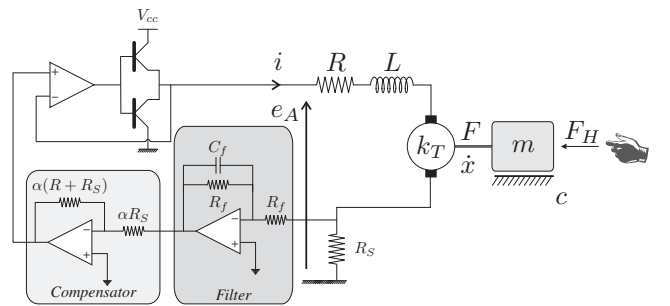


Fig. 5. Diagram of a simple position holding analog circuit

### IV. THE WAVE-HAPTICS APPROACH

Although providing important insights on the possibility for stiff encoderless force feedback, the simple circuit outlined in the previous section cannot be directly used in haptic interfaces since it lacks the capability of being programmed to render arbitrary virtual environments. On the other hand,

electrical currents and voltages provide information about the mechanical domain and such information is fully utilized by the circuit of Fig. 5. The current  $i$  indicates a measurement of the force  $F$ , while the voltage  $e_W$  can be reconstructed from  $e_A$  through the knowledge of motor resistance to provide a measurement of the velocity  $\dot{x}_W$ . To implement arbitrary virtual environments, the system has to allow us to program the input-output relation between  $i$  and  $e_W$ .

Furthermore, previous studies in the field of telerobotics [19], [20], showed that wave variables are a convenient setting to provide robustness to time delays and time discretization. In view of these considerations, we interpret the motor resistance as part of a natural wave transform, as shown in Fig. 6. A wave transform encodes, without loss of information, the normal power variables of velocity and force into wave variables  $u$  and  $v$ . According to [20], wave variables are given here by:

$$\begin{aligned} v(t) &:= \frac{e_W - Ri}{\sqrt{2R}} = \frac{B_R \dot{x}_W - F}{\sqrt{2B_R}} \\ u(t) &:= \frac{e_W + Ri}{\sqrt{2R}} = \frac{B_R \dot{x}_W + F}{\sqrt{2B_R}} \end{aligned} \quad (10)$$

The equations on the right express the relationships between wave variables and equivalent mechanical quantities, where  $\dot{x}_W(t)$  is the desired motion and  $F$  is the common force applied by the spring  $K_L$  to the damper and to the rotor inertia  $m$ . The equivalent viscous damping  $B_R$  serves as the wave impedance.

The change of coordinates introduced by the wave transform (10) allows us to represent the overall instantaneous power  $P(t)$  flowing from the virtual environment to the controlled motor as:

$$P(t) = \dot{x}_W(t)F(t) = e_W(t)i(t) = \frac{1}{2}u^2(t) - \frac{1}{2}v^2(t) \quad (11)$$

Therefore each wave variable carries its own power content with  $u(t)$  encoding the power flowing into the motor and  $v(t)$  representing the power flowing from the motor into the virtual environment. In classical haptic systems, energetic inconsistencies that lead to instability arise because one power variable, typically the feedback force  $F$ , is the output of a time-discrete algorithm while the velocity changes during each sampling interval. Here, power flow is individually described by each wave variable independently of the other. System passivity depends only on the magnitudes of the wave variables and is hence unaffected by delays or lags.

To complete the wave transform, the dark shaded part of Fig. 6 consisting of the two  $\sqrt{2R}$  gains and the summing junction is realized by means of an *analog circuit*. In particular, the output voltage  $e_A$  is derived from current sensing as:

$$\begin{aligned} e_A(t) &= \sqrt{2R}u(t) \\ v(t) &= u(t) - \sqrt{2R}i(t) \end{aligned} \quad (12)$$

Because the wave variables  $u(t)$  and  $v(t)$  exist as electrical signals in the analog circuit, a passive implementation of the virtual environment can be obtained in several ways. First, simple transfer functions  $D(s) = U(s)/V(s)$  can be

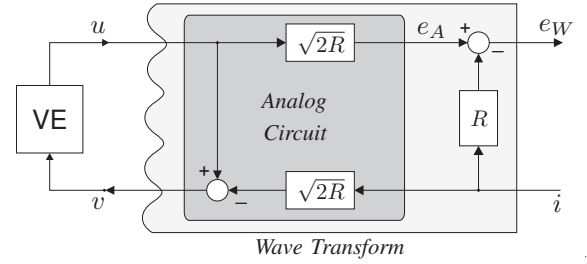


Fig. 6. The wave transform to interconnect the Virtual Environment (VE) to the electrical domain is implemented by means of an analog circuit.

realized in analog hardware. According to [19], their passivity is characterized as:

$$|D(s)| = \left| \frac{U(s)}{V(s)} \right| \leq 1 \quad (13)$$

Alternatively,  $v(t)$  and  $u(t)$  can be digitized and the virtual environment implemented on a computer either in wave space or in traditional power variables by use of a second decoding digital wave transformation. Energy consistency at the A/D interface is achieved if the sampled value  $v_h$  used in the digital virtual environment is such that:

$$T v_h^2 \leq \int_{(h-1)T}^{hT} v^2(\tau) d\tau \quad h \in \mathbb{N} \quad (14)$$

where  $T$  is the sampling period. Even though the performance evaluation of different discretization schemes is a matter of future investigation, we note that the condition (14) is satisfied if the integral of the input wave is sampled:

$$v_h = \frac{1}{T} \left| \int_{(h-1)T}^{hT} v(\tau) d\tau \right| \quad (15)$$

which suggests to take advantage of the low-pass characteristics of an anti-aliasing filter to ensure energy consistency at the interface between analog and digital loops.

Regardless of the specific implementation, any time delays or phase lags due to the discretization are guaranteed not to affect the stability of the overall system. Moreover, it is important to highlight that input to the virtual environment, corresponding to the wave signal  $v(t)$ , is not affected by limited position resolution as in the classical approach.

## V. HAPTIC INTERACTION THROUGH WAVE VARIABLES

By compensating for motor resistance, the wave-haptics circuit of Fig. 6, allows us to directly control the velocity  $\dot{x}_W$  at the end-point of the spring  $K_L$ , as shown in Fig. 7. This latter element therefore acts as coupler between the user and the virtual environment implemented in wave variables. Though similar to the virtual coupling concept of [24], here the coupling spring has the advantage of being a physical element, so it is not affected by the stability issues of a digital implementation.

The two most demanding virtual environments are free motion and perfectly rigid contact. Both imply an infinite frequency response (i.e. they are purely algebraic systems), as motion occurs immediately for any force in the former and

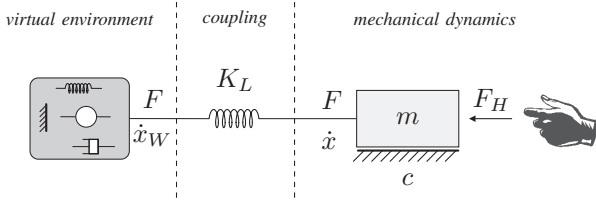


Fig. 7. Motor inductance acts as *physical* coupling with the virtual environment

forces are immediately created for any motion in the latter. These two virtual environments constitute the basis of every haptic display; the causality of an impedance device, designed to be light and back-driveable, clearly favors free motion and challenges rendition of rigid contact. Free motion avoids all forces ( $F = 0$ ) and reflects all power carried by the incoming wave  $v(t)$  back by means of  $u(t)$  as:

$$u(t) = v(t) \iff i = 0 \quad \forall e_W \iff F = 0 \quad \forall \dot{x}_W \quad (16)$$

where (10) is used to convert between wave and power variables. Dually, a rigid contact also reflects all power by suppressing any motion ( $\dot{x}_W = 0$ ):

$$u(t) = -v(t) \iff e_W = 0 \quad \forall i \iff \dot{x}_W = 0 \quad \forall F \quad (17)$$

Note that this does not hold the applied voltage  $e_A$  at zero, but only cancels the voltage across the inductor and back-EMF. It does not short the motor; instead it effectively sets  $e_A = Ri$  as seen in Sect. III. Therefore, in this situation  $K_L$  is the maximum stiffness that can be rendered to the user.

#### A. Analog Implementation of the Unilateral Wall

In order to evaluate the performance of the wave-haptics scheme, we use analog hardware to implement the transfer functions corresponding to free space (16) and to rigid contact (17). A collision detection algorithm based on direct position measurements generates a logical signal

$$\delta_{\text{FREE}}(x) = \begin{cases} 0 & x < 0 \\ 1 & x \geq 0 \end{cases} \quad (18)$$

that commands the switching between the two environments to simulate a virtual rigid wall with unilateral constraint:

$$u(t) = \eta(x)v(t) \quad \text{where} \quad \eta(x) = -1 + 2\delta_{\text{FREE}}(x) \quad (19)$$

Note however that the encoder is not used to directly compute the force fed back to the user.

When incorporating and utilizing the electrical dynamics,  $K_L$  is the maximum stiffness that can be rendered by means of a passive wave-haptic approach. Disturbances may stem from the unmodeled high frequency dynamics of the power transistors used to achieve the desired voltage input  $e_A$ , as well as from other sources of electrical noise in the control loop. However, these phenomena occur at much higher frequencies (several hundred kilohertz) than the perceptual bandwidth of the human operator (about one kilohertz). Consistent with Fig. 5, a high frequency low-pass wave filter:

$$H(s) = \frac{\lambda}{s + \lambda} \quad (20)$$

can then be included in series with the virtual environment to address these limitations without significantly affecting the perceived transients [25]. Such a filter attenuates the high frequency content of the wave variables and, because of (11) and (13), it corresponds to a frequency dependent power dissipation.

The transfer function  $D(s)$  of the overall controller dynamics in the wave domain becomes:

$$D(s) = \frac{U(s)}{V(s)} = \eta(x) \frac{\lambda}{s + \lambda} \quad (21)$$

where the magnitude of  $\eta$  can be further tuned in the interval  $-1 \leq \eta \leq 1$  to remove power and introduce damping.

## VI. COMPARISON TO THE CLASSICAL APPROACH

The root locus analysis allows to compare the stability characteristics of the wave-haptics approach to the traditional schemes built upon current amplifiers and encoder feedback.

In particular, a traditional current amplifier aims at speeding up the motor electrical pole while rejecting the back-EMF voltage. Usually [26] this is achieved through a PI current regulator:

$$E_A(s) = k_A \frac{\tau_A s + 1}{\tau_A s} [I_c(s) - I(s)] \quad (22)$$

being  $I_c(s)$  the commanded current set-point. As shown by the root locus of Fig. 8(a), the time constant  $\tau_A$  is chosen to be moderately faster than the motor electrical pole  $-R/L$ . A positive proportional gain  $k_A$  has then the effect to speed up the overall electrical dynamics, while the integrator ensures back-EMF rejection at low frequencies. On the top of the current regulator (22), force feedback is obtained by closing a loop around the measured device position  $x$ :

$$F_c(s) = k_T I_c(s) = K_c [X_c(s) - X(s)] \quad (23)$$

where  $K_c$  is the assigned stiffness and  $X_c(s)$  is the position of the virtual wall. The corresponding root locus, Fig. 8(b),

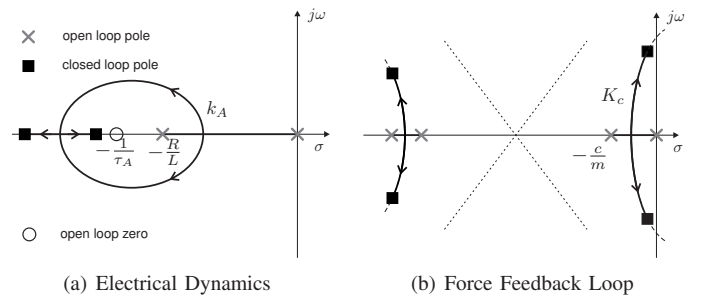


Fig. 8. Root locus interpretation of the classical approach

shows that for high force feedback gains  $K_c$  the mechanical poles tend to move to the right half-plane. Mechanical friction  $c$  (here considered linear for simplicity), becomes crucial to ensure stable operation, even neglecting the fact that (23) is usually implemented as a digital control loop, and thus time discretization and position quantization further limit the maximum achievable gain  $K_c$ .

To derive the root locus corresponding to the wave-haptics scheme defined by (12) and (21), we consider the analog circuit of Fig. 6 to have a tunable gain  $R_0$  that, in the ideal case, matches motor resistance  $R$ . Hence the electrical dynamics in the wave-haptics controller are:

$$E_A(s) = -2R_0 \frac{D(s)}{1 - D(s)} I(s) \quad (24)$$

In the case of stiff contact ( $\eta = -1$ ) and with the wave filter (20) this simplifies to:

$$E_A(s) = R_0 \frac{2\lambda}{s + 2\lambda} I(s) \quad (25)$$

As shown in Fig. 9(a), the pole related to the wave filter  $H(s)$  is moved to  $-2\lambda$ ; because of positive feedback used by the wave-haptics circuit, closed loop poles move outward, with the electrical pole of the motor reaching a pure integrator  $1/(Ls)$  as  $R_0 \rightarrow R$ . The dynamics relating motor current to position and velocity are considered in Fig. 9(b). Since we did not attempt to cancel the motor back-EMF, its effect is then to close, with fixed feedback gain  $k_T^2$ , a loop between the mechanical pole  $-c/m$  and the aforementioned integrator, thus providing a stiff behavior. Moreover, the wave filter  $H(s)$

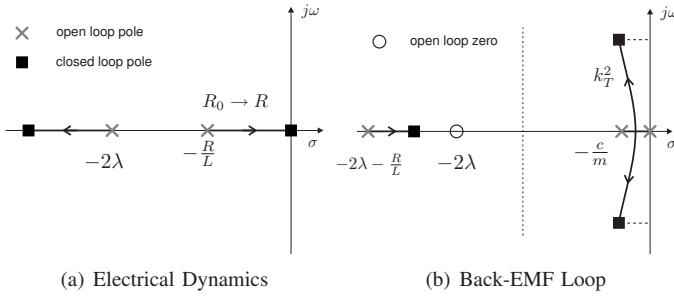


Fig. 9. Root locus interpretation of the wave-haptics controller for stiff contact ( $\eta = -1$ )

introduces an additional zero at  $-2\lambda$  that attracts the high frequency pole, while slightly moves to the left the oscillatory poles, thus improving their stability regardless of mechanical friction. This agrees with the fact that the overall system has to be passive, since both the motor dynamics and the wave filter  $H(s)$  are passive. Finally, note that no explicit loop involving position sensing is required for force feedback and the resulting system has relative degree 2. For comparison, the traditional loop closure has relative degree 4 and is therefore more difficult to stabilize for high gains  $K_c$ . Note that in both cases, dynamics of power transistors have been neglected.

In the case of free space ( $\eta = 1$ ), the electrical dynamics (24) simplify to:

$$E_A(s) = -2 \frac{R_0 \lambda}{s} I(s) \quad (26)$$

and the wave haptic controller acts as an integral controller that regulates the current to zero, and can be interpreted as a mass attached to the motor in a similar way to the PI controller (22). With respect to the traditional approach, we notice that oscillatory high frequency poles are left non compensated. Even though this parasitic behavior appears at a frequency

beyond the human perceptual bandwidth, it can be minimized through a suitable choice of the time constant  $\lambda$  of the wave filter.

## VII. ROBUSTNESS AND ABSOLUTE POSITION FEEDBACK

Because of thermal effects during motor operation,  $R$  can increase by about 20% of its nominal value, thus making the perfect compensation of motor resistance  $R$  very difficult in practice.

As suggested by the previous root locus analysis, robustness and passivity of the control scheme are retained only if the motor resistance  $R$  is compensated only up to a certain fraction  $R_0$ , allowing for a positive uncompensated residual  $\rho = R - R_0 \geq 0$ . In mechanical terms, the residual electrical resistance  $\rho$  maps into a viscous damper:

$$B_\rho = \frac{k_T^2}{\rho} > 0 \quad (27)$$

that is connected in series with the spring  $K_L$ . This situation is sketched in Fig. 10, where we note that the velocity  $\dot{x}_\rho$  of the spring endpoint differs from the velocity  $\dot{x}_W$  controlled by the wave-haptics circuit:

$$\dot{x}_\rho = \dot{x}_W - \frac{1}{B_\rho} F \quad (28)$$

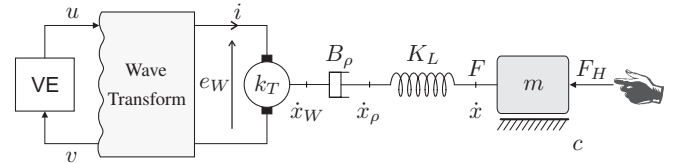


Fig. 10. The uncompensated residual resistance  $\rho$  maps into a mechanical damper  $B_\rho$ . The wave circuit does not directly control the spring endpoint  $x_\rho$ .

Although the wave-haptics circuit is able to exploit the stiff behavior at frequencies lower than the natural frequency  $R/L$  of the motor electrical pole, the presence of the residual damper  $B_\rho$  is responsible for the viscous behavior at frequencies up to  $\rho/L < R/L$ . At these frequencies, the spring endpoint  $x_\rho$  may slowly drift from the desired position  $x_W$ .

Recovering the cascaded loop closure outlined in Fig. 1, absolute position feedback is used in a digital control loop to provide the low frequency performances during the contact with a stiff virtual object. Since motor inductance  $L$  and torque constant  $k_T$  are relatively more stable in temperature than the resistance  $R$ , an estimate of the spring end-point position  $x_\rho$  can be derived as:

$$x_\rho = \frac{L}{k_T} i + x \quad (29)$$

where  $i$  and  $x$  are gathered through position and current sensors. A wave signal  $u_P(t)$  is computed by a discrete time algorithm according to the simple proportional law:

$$u_P = P [x_{sp} - x_\rho] \quad (30)$$

where  $P$  is the proportional gain and  $x_{sp}$  is the desired position for the endpoint  $x_\rho$ . Finally  $u_P$  is summed to the output of the analog circuit (12) to obtain:

$$U(s) = D(s)V(s) + H(s)U_P(s) \quad (31)$$

By comparing (30) to (10), the compensation wave can be interpreted as an elastic force that is added to  $F$  in (10) in order to guarantee that  $x_\rho$  reaches, at least in steady state, the desired position  $x_{sp}$ .

As noted in Sect. II, humans are particularly sensitive at frequencies about 200 Hz, while at lower frequencies the poor position resolution of the neuromuscular apparatus limits their ability to identify the rendered stiffness. Therefore the feedback gain  $P$  can be kept relatively small, thus avoiding the stability issues due to digital implementation [13]. This fact allows to substantially neglect the non-idealities of the digital implementation and to evaluate the behavior of the overall system in the time continuous domain.

### VIII. PERFORMANCE EVALUATION

In order to simplify system analysis, we assume  $x_{sp} = 0$  and neglect the wave filter  $H(s)$ , since it has been noted that it provides high frequency damping without significantly affecting performances in the frequency range of haptic interaction. Previous considerations allow to approximate the outer digital loop as a time continuous system.

In the case of stiff contact ( $\eta = -1$ ), the transfer function between the user input force  $F_H(s)$  and the feedback force  $F(s)$  is described as:

$$\frac{F(s)}{F_H(s)} = \frac{K_L B_\rho \left( s + P \sqrt{\frac{R_0}{2k_T^2}} \right)}{B_\rho \left( s + P \sqrt{\frac{R_0}{2k_T^2}} \right) (ms^2 + cs + K_L) + sK_L (ms + c)} \quad (32)$$

while device position  $X(s)$  is described as:

$$\frac{X(s)}{F_H(s)} = - \frac{B_\rho \left( s + P \sqrt{\frac{R_0}{2k_T^2}} \right) + K_L}{B_\rho \left( s + P \sqrt{\frac{R_0}{2k_T^2}} \right) (ms^2 + cs + K_L) + sK_L (ms + c)} \quad (33)$$

where  $c$  is the linearized mechanical friction. Therefore, the frequency dependent stiffness  $K(s)$  is:

$$K(s) = - \frac{F(s)}{X(s)} = \left[ \frac{1}{K_L} + \frac{1}{B_\rho \left( s + P \sqrt{\frac{R_0}{2k_T^2}} \right)} \right]^{-1} \quad (34)$$

In other words, the total stiffness  $K(s)$  is given by the parallel connection of the electrical stiffness  $K_L$  and the spring generated by the digital controller. In particular, in the case of ideal compensation ( $\rho \rightarrow 0$  and  $B_\rho \rightarrow \infty$ ), the electrical stiffness  $K_L$  is active at all frequencies. On the other hand, it is clear that without digital controller ( $P=0$ ), the residual viscous damping  $B_\rho$  dominates at low frequencies, causing the position (33) to drift. This phenomenon is finally compensated by the gain  $P$ , that, together with the wave gain  $R_0$ , determines the bandwidth and the stiffness of the low-frequency spring:

$$K_P = B_\rho \sqrt{\frac{R_0}{2k_T^2}} P = \frac{B_\rho}{\sqrt{2B_0}} P \quad (35)$$

Note that this stiffness depends on  $B_\rho$  and is sensitive to parametric uncertainties on  $\rho$ . Previous considerations on user's perception suggest however that such uncertainty can be tolerated.

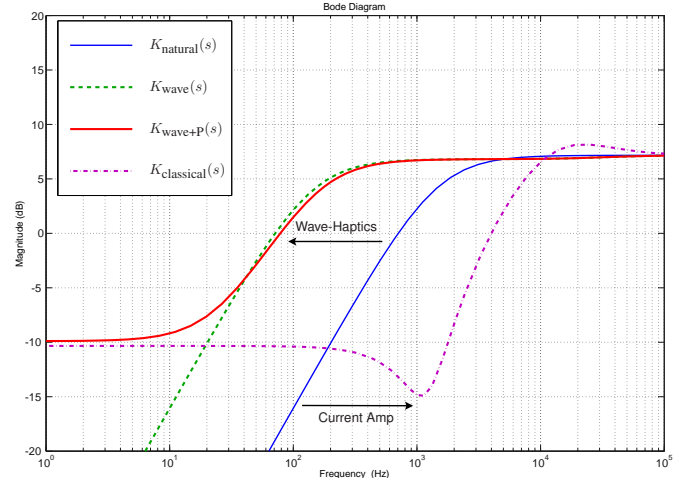


Fig. 11. Bode diagrams comparing the wave-haptics and the classical controllers in the case of stiff contact.

The behavior of the wave-haptics controller can be best viewed by means of Bode plots. In particular, Fig. 11 compares the stiffness (34) rendered by different control schemes in the case of rigid contact. Plots are derived from the parameters of the Maxon RE25-118743 motor used for experiments in the next section. Although neglected in the analytic derivations, a wave filter (20) with  $\lambda = 100,000$  rad/sec is considered in the plot.

First, the natural behavior  $K_{natural}(s)$  of a DC motor when  $e_A = 0$  (solid thin line) exhibits, as expected, a flat behavior with magnitude  $K_L$  at high frequency, normally beyond the bandwidth of human kinesthetic perception. Lower frequencies are dominated by electrical dissipation.

When stiff contact (17) is simulated, the analog circuit (12) actively compensates for motor resistance. As shown by the curve  $K_{wave}$  (dashed) with  $R_0 = 0.9R$ , the analog circuit shifts the region of high stiffness to the range of frequencies corresponding to human sensitivity peak. Residual low frequency attenuation is then compensated by the proportional controller (30), as illustrated by the curve  $K_{wave+P}$ .

For comparison, the dash-dotted line represents the behavior of the traditional haptic controller as described by (22) and (23). The curve labeled  $K_{classical}(s)$  shows how current amplifiers are designed to speed up the motor electrical pole while rejecting back-EMF through an high feedback gain eventually provided by an integrator. By recalling (3), the digital loop directly commands the feedback force on the basis of the measured position displacement. Hence in the traditional scheme the region exhibiting electrical stiff behavior is shifted to an even higher frequency. The digital force feedback loop, approximated here as a continuous-time system, is thus required to provide stiff behavior over the whole frequency range of human kinesthetic perception. When high stiffnesses are rendered, quantization and discretization

effects become non-negligible at frequencies about the human sensitivity peak and stability issues arise [13].

The advantage of the wave-haptics approach is therefore to use digital control in a range of frequencies that falls within its capabilities with usual servo rates and position resolution. The physical spring  $K_L$  naturally provided by the motor is retained to achieve stable stiff kinesthetic interaction at high frequencies.

The corresponding Bode diagrams for the free motion ( $\eta = 1$ ) are illustrated in Fig. 12. Analogously to Fig. 12, a wave filter (20) with  $\lambda = 100,000$  rad/sec is considered to derive the plots. In this case the difference between the wave-haptics scheme and the traditional controller is relatively modest; both approaches build a current loop that contains an integral effect. On the other hand, the presence of a proportional term in the traditional controller (22) filters the resonant peak that otherwise appears in the wave-haptics plots. This effect is located at frequencies well beyond the human perceptual capabilities and experiments suggest that it can be tolerated. Further investigations are required to optimize wave filter design minimizing the resonant peak. Finally note that the curves  $K_{wave}$  and  $K_{wave+P}$  are almost coincident, thus the proportional controller (30) can be turned off when simulating free space.

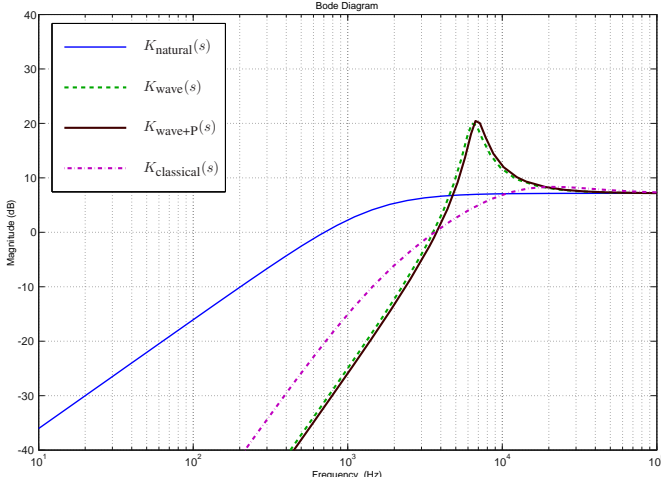


Fig. 12. Bode diagrams comparing the wave-haptics and the classical controllers in the case of free motion.

## IX. IMPLEMENTATION AND EXPERIMENTS

We have realized a simple prototype system that extends the scheme of Fig. 5, allowing to implement the control equations (21), (30) (31) with  $\lambda = 100,000$  rad/sec,  $\eta = \pm 1$ . The block diagram of the overall system is sketched in Fig. 13.

In particular, the user grasps an handle mounted at the shaft of a Maxon RE25-118743 motor that features  $K_L = 2.2815$  Nm/rad, similar to the electrical stiffness of motors commonly found in PHANToM devices. Power amplification is performed by a couple of complementary MOSFET transistors in a push-pull configuration and an analog switch alternates between free space ( $\eta = 1$ ) and rigid contact ( $\eta = -1$ ). Data is collected at 5 KHz using A/D conversion and a

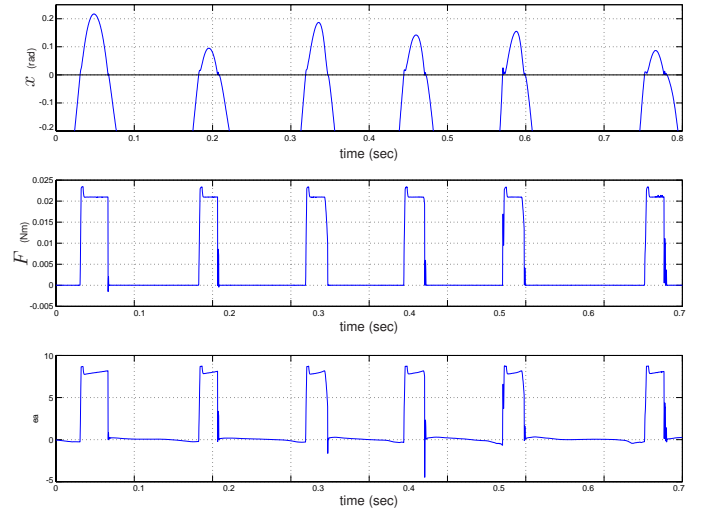


Fig. 14. Repeated contacts with the virtual wall: position, force and voltage diagrams -  $P = 0$

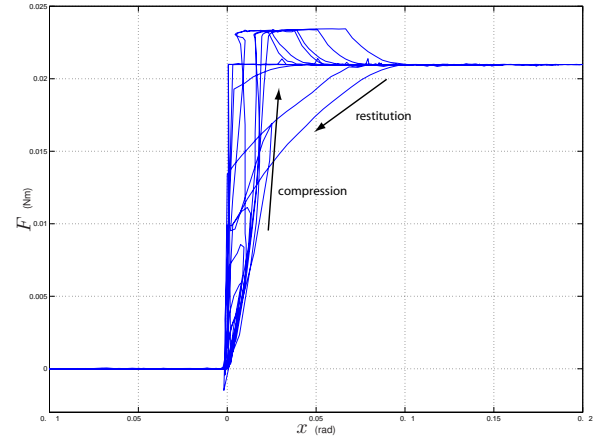


Fig. 15. Behavior of the feedback torque  $F$  during contact with the virtual wall -  $P = 0$

high resolution encoder ( $10^4$  counts per revolution) to measure the motor shaft position, while the proportional compensation (30) and the collision detection (19) are computed using a more realistic servo rate of 1 KHz and a position resolution of 2,000 counts per revolution. The location of the virtual wall has been set to  $x_{sp} = 0$  for simplicity and contact is experienced for  $x \geq 0$ .

Preliminary results obtained for repeated impacts against the virtual wall are shown in Fig. 14 and 15. In these experiments the wave gain  $R_0$  has been tuned to match the motor resistance  $R$  with an error of less than 2%, while the proportional controller has been disabled (i.e.  $P = 0$ ). To limit thermal effects maximum current has been limited, through power supply, to 1 A. From Fig. 14 we see the circuit correctly renders the behavior of free space, since when  $x < 0$  the feedback torque  $F$  is zero. The voltage  $e_A$  adjusts slightly to counter the back-EMF voltage. As contact is experienced, current and torque quickly rise to their maximum value before saturation intervenes at about  $F \approx 0.021$  Nm. Better viewed in Fig. 15, the stiffness rendered during the compression phase

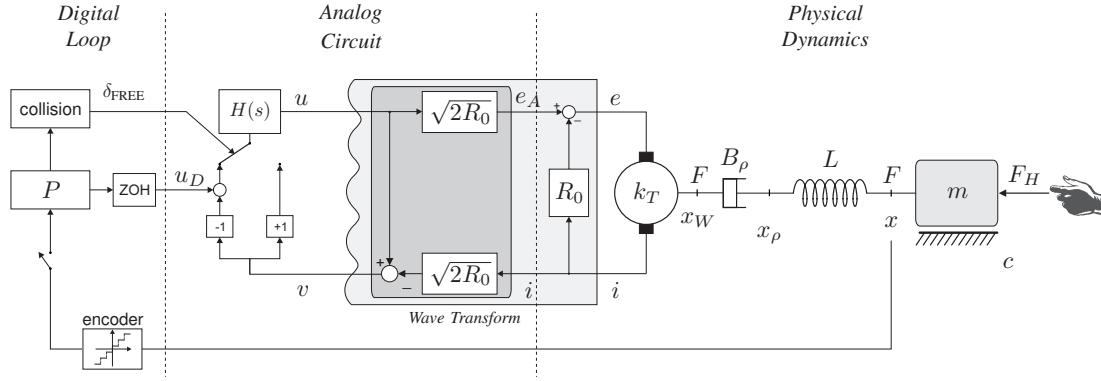


Fig. 13. The complete scheme for virtual wall simulation. Collision detection drives an analog switch that selects between free space and stiff contact. In this latter case, proportional digital controller compensates for residual damper  $B_\rho$ . The resulting voltage  $e_A$  is applied to the motor.

is approximately  $K \simeq 1.9$  Nm/rad, in good agreement with the expectations from the previous analysis.

We note that the compression and the restitution phases appear asymmetric. This behavior is a direct consequence of voltage saturation, which is not yet included in the simple dynamics (1). When the drive voltage hits a fixed saturation limit, the back-EMF effects can not be properly canceled and the current  $i$  is affected by motion. As the compression slows, the resisting force drops to its steady state value and, as motion begins during restitution, the restoring force drops accordingly. Effectively the spring forces are overlaid with the back-EMF's viscous damping.

Similarly to what noted in Sect. VII, the voltage modification caused by the saturation also shifts the endpoint  $x_\rho$  of the spring  $K_L$ , since the voltage  $e_A$  is not sufficient to achieve perfect compensation of the term  $Ri$ . Fortunately, as contact is broken, the behavioral switch via  $\eta$  resets the system for the next collision.

Previous experiments have been repeated in a more realistic situation, by tuning  $R_0 \simeq 0.9R$  and taking advantage of absolute position feedback. Moreover, current saturation has been increased to 1.85 A. In particular, results obtained with a low proportional gain so that  $K_P \simeq 0.02$  Nm/rad, are presented in Fig. 16 and Fig. 17. By looking at the latter diagram, we notice that the residual motor resistance causes an hysteresis loop to arise. The area encircled by compression and restitution phases corresponds to dissipated energy. Moreover, the compression phase is characterized by two different behaviors. Immediately after impact occurs, the high frequency stiffness provided by  $K_L$  dominates. Because of the proportional controller, the rendered stiffness decreases as a quasi-static regime is reached, with the user slowly moving the handle further into the virtual object.

The corresponding diagram obtained  $K_P \simeq 0.38$  Nm/rad is shown in Fig. 18. By increasing the gain of the digital controller we notice that compression and restitution phases generate almost overlapping diagrams. Therefore no energy generation occurs and the system is stable. Moreover, during the compression phase the digital controller is sufficient to prevent the spring endpoint  $x_\rho$  from drifting from the desired position. The rendered stiffness is in this case of about

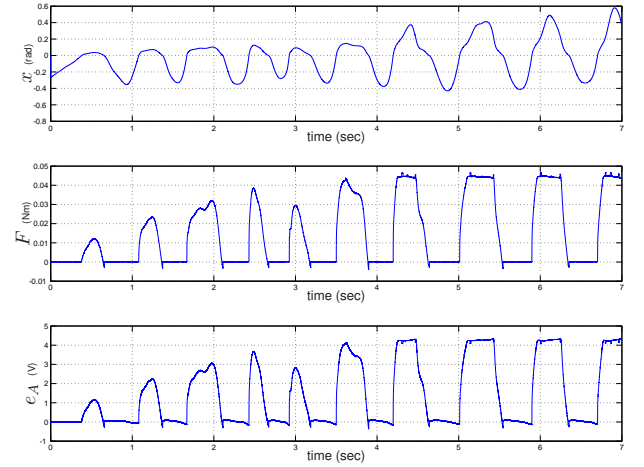


Fig. 16. Repeated contacts with the virtual wall: position, force and voltage diagrams -  $K_P \simeq 0.02$  Nm/rad

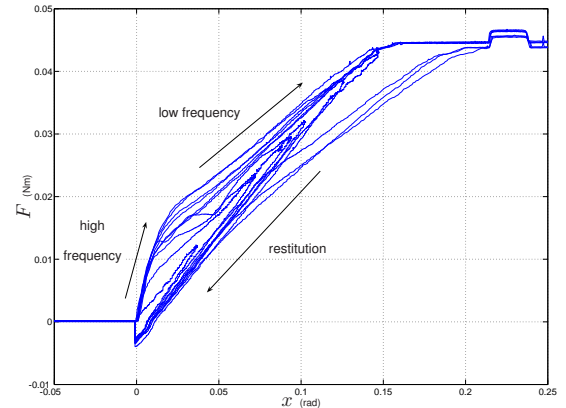


Fig. 17. Behavior of the feedback torque  $F$  during contact with the virtual wall -  $K_P \simeq 0.02$  Nm/rad

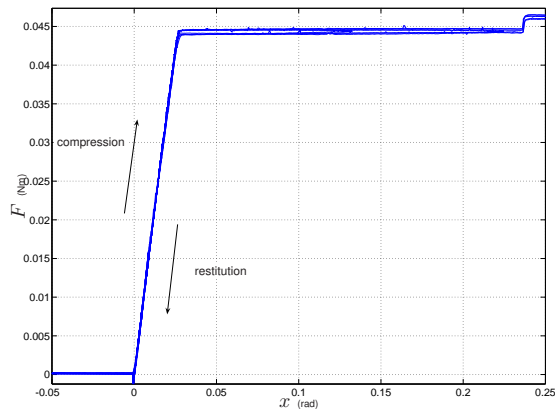


Fig. 18. Behavior of the feedback torque  $F$  during contact with the virtual wall -  $K_P \simeq 0.38$  Nm/rad

2 Nm/rad, in good agreement with theoretical expectations and about 7 times higher than the one obtained through traditional current amplification. After saturation occurs, the proportional controller enables the restitution phase to take place at the correct location.

As a final remark, both Fig. 17 and Fig. 18 exhibit a small discontinuity at about 0.22 rad. It corresponds to a motor brush commutation that is not filtered through the analog circuitry. Such discontinuities may be perceived by the user and the application to brushless motors promises smoother operation.

## X. CONCLUSIONS

In this paper we propose to exploit the electrical dynamics of DC motors to improve force feedback in virtual reality applications. With the motors commonly used in haptics, the equivalent stiffness provided by motor inductance is higher than the stiffness that can be achieved by means of a classical digital control loop and provides force feedback without requiring direct position sensing.

An analog circuit has been designed to replace traditional current amplifiers in order to exploit this effect. Wave variables are available as analog signals, facilitating the implementation of a passive and power consistent coupling to virtual environments.

As the physical inductance-based stiffness is available at all frequencies, the need for digital control loop is shifted to a lower frequency range, where quantization and discretization do not substantially affect system stability. As shown in Fig. 11, the system is able to render higher stiffnesses over the frequency range matching the human perceptual characteristics.

This approach is very appealing with its intrinsic simplicity and its better use of the physical components of the haptic device. It does not require assumptions on the mechanical friction to obtain stability and passivity. Conversely, the passivity is obtained constructively and the effects of non-idealities are confined behind the wave variables transform, guaranteeing intrinsic robustness to servo delay.

In future research activity, user studies will be carried out to validate the suitability and the effectiveness of the wave-haptics approach. Similarly to what presented in [13], further analysis will relate the gain of the digital controller (30) to system parameters and to parametric uncertainties on  $\rho$ . Moreover, the realization of more complex virtual environments as passive digital algorithms in wave domain will be studied analyzing different discretization techniques for the analog wave variables  $u(t)$  and  $v(t)$ . Finally, the extension to multi-DOF devices that require coordination between different motors will be investigated.

## REFERENCES

- [1] G. Niemeyer, N. Diolaiti, and N. Tanner, "Wave haptics: Encoderless virtual stiffnesses," in *ISRR 2005: International Symposium of Robotics Research*, San Francisco, CA, USA, October 2005.
- [2] N. Diolaiti and G. Niemeyer, "Wave haptics: Providing stiff coupling to virtual environments," in *Proceedings of the IEEE Symposium on Haptic Interfaces for Virtual Environment and Teleoperator Systems*, Washington D.C., U.S.A., March 2006.
- [3] K. Shimoga, "A survey of perceptual feedback issues in dextrous telemanipulation. part ii: finger-touch feedback," in *IEEE Annual Virtual Reality International Symposium*, 1993, pp. 271–279.
- [4] I. Darian-Smith, "The sense of touch: Performance and peripheral neural processes," in *Handbook of Physiology: The nervous system III*. Bethesda, MD: American Physiological Society, 1984, pp. 739–788.
- [5] R. Daniel and P. McAree, "Fundamental limits of performance for force reflecting teleoperation," *International Journal of Robotics Research*, vol. 17, no. 8, pp. 811–830, August 1998.
- [6] T. Massie and J. Salisbury, "The phantom haptic interface: a device for probing virtual objects," in *ASME Winter Annual Meeting*, vol. 55-1, New Orleans, LA, 1994, pp. 295–300.
- [7] D. Lawrence, L. Pao, A. Dougherty, M. Salada, and Y. Pavlou, "Rate hardness: A new performance metric for haptic interfaces," *IEEE Transactions on Robotics and Automation*, vol. 16, no. 4, pp. 357–371, August 2000.
- [8] Y. Koren and A. Ulsoy, "Control of DC servo-motor driven robots," in *Proceedings of Robot 6 Conference*, SME, Ed., Detroit, March 1982.
- [9] J. Colgate and G. Schenkel, "Passivity of a class of sampled-data systems: Application to haptic interfaces," in *American Control Conference*, Baltimore, Maryland, June 1994, pp. 3236–3240.
- [10] B. Gillespie and M. Cutkosky, "Stable user-specific rendering of the virtual wall," in *ASME IMECE*, vol. DSC-Vol. 58, Atlanta, GA, November 1996, pp. 397–406.
- [11] M. Mahvash and V. Hayward, "High fidelity passive force reflecting virtual environments," *IEEE Transactions on Robotics*, vol. 21, no. 1, pp. 38–46, 2004.
- [12] J. J. Abbott and A. M. Okamura, "A sufficient condition for passive virtual walls with quantization effects," in *ASME IMECE International Symposium on Advances in Robot Dynamics and Control*, Anaheim, CA, USA, Nov. 2004, pp. 1065–1073.
- [13] N. Diolaiti, G. Niemeyer, F. Barbagli, J. K. Salisbury, and C. Melchiorri, "The effect of quantization and coulomb friction on the stability of haptic rendering," in *WHC '05: First WorldHaptics Conference*. Pisa, Italy: IEEE Computer Society, March 2005, pp. 237–246.
- [14] B. Hannaford and J. Ryu, "Time domain passivity control of haptic interfaces," in *Proceedings of the IEEE International Conference on Robotics and Automation*, Seoul, Korea, May 2001, pp. 1863–1869.
- [15] M. Kawai and T. Yoshikawa, "Haptic display with an interface device capable of continuous-time impedance display within a sampling period," *IEEE/ASME Transactions on Mechatronics*, vol. 9, no. 1, pp. 58–64, March 2004.
- [16] J. Colgate and J. Brown, "Factors affecting the z-width of a haptic display," in *Proceedings of the IEEE International Conference on Robotics and Automation*, San Diego, CA, May 1994, pp. 3205–3210.
- [17] J. S. Mehling, J. E. Colgate, and M. A. Peshkin, "Increasing the impedance range of a haptic display by adding electrical damping," in *WHC '05: First WorldHaptics Conference*. Pisa, Italy: IEEE Computer Society, March 2005, pp. 257–262.
- [18] J. Fiene and G. Niemeyer, "Switching motor control: An integrated amplifier design for improved velocity estimation and feedback," in *Proceedings of the IEEE International Conference on Robotics and Automation*, vol. 5, New Orleans, LA, USA, April 2004, pp. 4504–4509.

- [19] G. Niemeyer and J. Slotine, "Using wave variables for system analysis and robot control," in *Proceedings of the IEEE International Conference on Robotics and Automation*, vol. 2, Albuquerque, New Mexico, April 1997, pp. 1619–1625.
- [20] —, "Telem Manipulation with time delays," *International Journal of Robotics Research*, vol. 23, no. 9, pp. 873–890, September 2004.
- [21] S. Stramigioli, A. van der Schaft, B. Maschke, and C. Melchiorri, "Geometric scattering in robotic telemanipulation," *IEEE Transactions on Robotics and Automation*, vol. 18, no. 4, 2002.
- [22] H. Paynter, *Analysis and Design of Engineering Systems*, ser. Class 2.571. M.I.T. Press, 1960.
- [23] D. C. Karnopp, D. L. Margolis, and R. C. Rosenberg, *System Dynamics: Modeling and Simulation of Mechatronic Systems*, 3rd ed. John Wiley and Sons, 2000.
- [24] B. Miller, J. Colgate, and R. Freeman, "Environment delay in haptic systems," in *Proceedings of the IEEE International Conference on Robotics and Automation*, San Francisco, CA, April 2000, pp. 2434–2439.
- [25] N. Tanner and G. Niemeyer, "Practical limitations of wave variable controllers in teleoperation," in *IEEE Conference on Robotics, Automation, and Mechatronics*, Singapore, 1-3 December 2004.
- [26] W. Leonhard, *Control of Electrical Drives*, 3rd ed. Berlin: Springer Verlag, 2001.